CrystEngComm



PAPER



Cite this: CrystEngComm, 2022, 24, 1891

Stereo-electronic effect of the perfluoropropyl group on the solid-state molecular packing of isomeric dibenzo[a,c]phenazine derivatives†

Anjaneyulu Putta, D Shankar Gairhe, Yao Feng and Haoran Sun D*

We report here the synthesis, characterization, and crystal structures of three perfluoropropylated dibenzo[a,c]phenazine constitutional isomers, in which the only difference among them was the positions of the perfluoropropyl substituents. The crystal structures of these perfluoropropylated dibenzo[a,c] phenazine isomers indicated that the stereo-electronic effect of the perfluoropropyl group on the dibenzo[a,c]phenazine molecule plays a crucial role in determining the crystal-packing motif in the solid state. Our results from both X-ray crystallography and computational approaches revealed that the positions of the perfluoropropyl groups on the dibenzo[a,c]phenazine ring significantly affected the electrostatic potential distribution along the aromatic ring surface, resulting in drastic changes in the molecular packing in the solid state, from herringbone to lamellar crystal packing, among these three constitutional isomers. Simple topological consideration of the molecular packing in the solid state was coincidently cooperative with the changes in the electrostatic potential distributions, where localized partial positive and partial negative charges perhaps dominated the intermolecular interactions between the aromatic rings. Together, the perfluoropropylation on the dibenzo[a,c]phenazine ring provided us with a fortunate scenario, wherein the molecular topological structure and electrostatic potential worked together to facilitate the formation of the desired lamellar π - π stacked crystal packing. Meanwhile, electrochemistry, UV-visible absorption and emission spectra, and the computational chemistry results pointed out that there were only minor to moderate changes in the electronic properties of the molecules upon changing the position of the perfluoroalkylation on the dibenzo[a,c]phenazine core. While controlling the solid-state structure of aromatics by design still has a long way to go, we hope that our work will ignite a spark that can potentially spread into the field of the design of organic solid-state materials.

Received 6th January 2022, Accepted 30th January 2022

DOI: 10.1039/d2ce00019a

rsc.li/crystengcomm

1 Introduction

Despite the recent advancement of organic semiconductor materials, 1,2 designing new, small molecular organic semiconductor materials with a predictable crystal-packing motif and electronic properties is still a significant challenge, 3,4 due to the coexisting weak intermolecular interaction forces, which are often only a few kcal mol $^{-1}$ at most. 5,6 Modification of the molecular structure of organic semiconductors, *i.e.* making changes in the size of π conjugation, 7,8 changes in substitution of the π

Department of Chemistry and Center for Fluorinated Functional Materials, University of South Dakota, Vermillion, South Dakota, 57069, USA. E-mail: Haoran.Sun@usd.edu

† Electronic supplementary information (ESI) available: Synthetic procedures and characterization data of compounds 1 and 3, crystal structure analysis results, computational chemistry procedures and coordinates of optimized geometries and total energies of compounds 1, 2, and 3. CCDC 2053442–2053444. For ESI and crystallographic data in CIF or other electronic format see DOI: 10.1039/d2ce00019a

conjugation, $^{9-11}$ and doping of hetero-atoms into the π conjugation, $^{12-14}$ generally provides predictable changes in the electronic properties at the molecular scale. However, such modification at the molecular level often results in unpredictable electronic properties for the bulk materials, where such properties are governed by the structures at both the molecular and bulk solid-state levels. 15,16 For example, molecules with the same size/shape π system but different substituents can display drastic differences in their electronic properties due to the differences in the molecular packing motifs in the solid state. 17,18

The crystal-packing mode in organic semiconductor materials can be altered through several strategies, though these are mostly still at the trial-and-error stage. $^{19-21}$ Generally, molecules with an ionic and/or coordination binding ability often show better capability in forming the desired solid-state packing in a controllable fashion. 22,23 However, the introduction of charged species and/or metal ions will likely significantly alter the electronic properties of the original π system used in such materials, though this

Paper CrystEngComm

may show significant benefits in other applications, such as catalysis and energy storage. 24,25 Another widely used approach is to utilize a strong hydrogen bonding network to build a desired solid-state molecular packing motif, with many successful cases reported involving controlling semiconductors' properties. $^{26-28}$

In the meantime, many promising organic semiconductor molecules lack the ability to form such a hydrogen bonding network or face significant challenges to do so.^{29–31} The solid-state structures of these types of organic semiconductors are controlled by intermolecular noncovalent bonding, including dipole–dipole, quadrupole–quadrupole, dipole–quadrupole, dipole and induced-dipole interactions.^{32,33} While these weak non-covalent bonding interactions are typically electrostatic in nature, prioritizing one type over the others among these non-covalent intermolecular interactions is key towards controlling the solid-state structures in the bulk to achieve control of the electronic properties of the bulk organic semiconductor materials.^{34–36}

Introducing electron-withdrawing groups onto aromatics is one of the strategies to control the crystal packing of organic semiconductor materials in the solid state. 37-40 The perfluoroalkyl group is one of the most versatile electronwithdrawing groups that is often added onto aromatic cores to improve the air-41-44 and photo-stability of aromatic molecules. 45-48 Molecular orbitals and their energy levels are also modulated by adding perfluoroalkyl groups to aromatic molecule. 49,50 Over the past, we identified that the localization of partial charges along the π system surface, represented by the differences in the molecular electrostatic potential (ESP) maps, plays a key role in controlling the molecular packing among the dibenzo [a,c] phenazine derivatives.⁵¹ Among the perfluoroalkyl substitutions (typically *n*-perfluorobutyl substituent) on the aromatic ring, we were able to achieve a lamellar π - π stacked molecular packing motif with less than a 3.4 Å interplanar distance in the solid state.

In addition to the strategies used in our previous work, 52,53 including the introduction of perfluoroalkyl substituents, increasing the size of π conjugation, and the introduction of highly polarizable soft hetero-atoms into the π system, we thought to purposely introduce perfluoroalkyl substituents onto different positions of the π system to create isomers that possess the same substituents and the π system. The only difference between these constitutional isomers is the position of the substitution. This approach provides us an opportunity to probe how the substitution position can affect the electronic properties of the large π system, an analogue question to the benchmark benzene derivatives, ortho and para vs. meta effects, and more importantly, how it would further extend its stereoelectronic properties to influence the molecular packing in crystal structures.

Here, we chose a medium-sized dibenzo[a,c]phenazine ring as the π system for our study due to its electron-

accepting capability and planar structure.⁵⁴ Moreover, dibenzo[a,c]phenazine is used as a promising n-type building block in the research and development of organic semiconductor materials, ranging from OLEDs, to solar cells, catalysts, and phototransistors.^{55–58} Despite their potential applications in the organic semiconductor field, research on the crystal structure and analysis of the crystal packing of dibenzo[a,c]phenazine derivatives have been scarcely reported.^{59,60}

Built on the foundation of our earlier work on perfluoroalkylated polyaromatic hydrocarbons (PAHs), $^{51-53,61}$ we report here the synthesis, characterization, and crystal structures of three isomers of perfluoropropylated dibenzo[a, c]phenazine. Together with the DFT calculation results, we further discuss the stereo-electronic effects of the perfluoroalkyl group on both the crystal packing and electronic properties of these three isomers (Chart 1).

2 Results and discussion

2.1 Synthesis

For the synthesis of compound 1, first 10,13-dibromo dibenzo[a,c]phenazine (PBrDBP) was synthesized from the condensation of 3,6-dibromo-1,2-phenylene diamine with 9,10-pheanthrenequiinone. Then, compound synthesized from 10,13-dibromo dibenzo [a,c] phenazine via a copper-mediated cross-coupling reaction perfluoropropyl iodide and Cu powder in a 54% yield, as shown in Scheme 1. Compound 2 was prepared by reacting *n*-perfluoropropyl iodide with 11,12-dibromo dibenzo[a,c] phenazine in the presence of Cu powder in a mixture of solvents DMSO and HFE-7200 with a 13% yield. The intermediate 11,12-dibromo dibenzo[a,c]phenazine was prepared by the condensation of 4,5-dibromo-1,2-phenylene diamine with 9,10-phenanthrene quinone. The synthetic method used for compound 3 was not attempted for the preparation of compound 2 as the synthesis 4,5-bisperfluoropropyl-1,2-phenylene diamine involves multiple synthetic steps and challenges for it to be synthetically successful. Compound 3 was synthesized modified procedure using a from our previously reported method. First, the key intermediate 3,6-bisperfluoropropylphenanthrene-9,10-dione synthesized from 3,6-dibromophenanthrene-9,10-di(ethylene

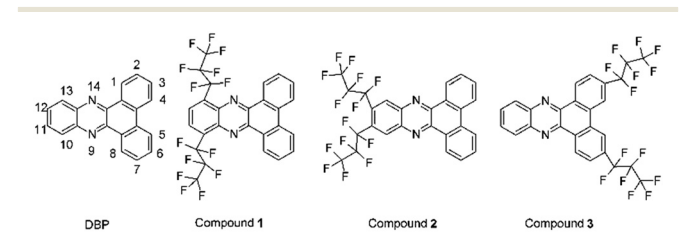


Chart 1 Molecular structures of the compounds in this study. Dibenzo[a,c]phenazine (DBP) with ring numbering and compounds 1–3. DBP is a commercial compound and compound 2 was reported in our previous work.

CrystEngComm Paper

Scheme 1 Reaction schemes for the synthesis of compound 1 (a), and compound 3 (b).

glycol)ketal, followed by perfluoropropylation and deprotection of the ketal. A condensation reaction between 3,6-bisperfluoropropylphenanthrene-9,10-dione and 1,2-phenylene diamine gave compound 3 in a 95% yield.

2.2 Effect of the *n*-perfluoropropyl groups' position on the crystal packing: crystal structure analysis

Single crystals of compound 1 were obtained by a slow evaporation of saturated dichloromethane solution for several days. Single crystals of compound 3 suitable for X-ray diffraction were obtained by a layered liquid-liquid diffusion method. First, a concentrated solution of compound 3 in dichloromethane was prepared and methanol was added carefully on top of the dichloromethane solution along the side wall of the small vial. The small vial was sealed and put in a quiescent place to avoid strong vibration for several days to yield light-yellow needle crystals. Compound 1 crystallized in the monoclinic system with the space group P21/c, while compound 3 crystallized in the monoclinic system with the space group C2/c.

Analysis of single-crystal structures, crystal-packing mode, and non-covalent interactions is of great importance to understand the electronic properties of organic materials. The crystal packing of unsubstituted dibenzo [a,c] phenazine (DBP) showed a herringbone pattern with minimal π - π overlapping between the aromatic rings. Upon adding the n-perfluoropropyl group on the parent dibenzo [a,c] phenazine aromatic ring at the 10,13-positions (compound 1), the crystal packing showed a herringbone pattern similar to the pattern in the unsubstituted dibenzo[a,c]phenazine (DBP). While changing the substitution position of *n*-perfluoropropyl group on dibenzo[a,c]phenazine from the 10,13-position to the 11,12-position (compound 2), the crystal packing changed to lamellar, though with some imperfection. When the *n*-perfluoropropyl groups were added onto the

3,6-positions (compound 3), the crystal packing was dramatically changed from herringbone to a perfect lamellar pattern. This change in crystal packing was due to the decrease in intermolecular interactions in C···H, F···C and the increase in C···C in the case of compound 3, which lead to the lamellar packing. Substitution at the 10,13-position (compound 1) resulted in a slipped face-face stacking with overall herringbone packing. While substitution of the n-perfluoropropyl groups at the 11,12-position (compound 2)⁵¹ and 3,6-position (compound 3) resulted in an antiparallel mode with overall lamellar packing. The π overlapping area decreased in the case of compound 1 compared to compounds 2 and 3. Due to the slipped parallel packing, only a portion of aromatic rings overlapped in compound 1, which can be seen from Fig. 1.

Slight changes in the interplanar distance among these three isomers were observed. With the presence of the *n*-perfluoropropyl group at the 11,12-position in compound 2, the π - π distance between two adjacent molecules was 3.379 Å, which was the largest π - π distance among all the isomers this study. By changing the position of the *n*-perfluoropropyl groups to the phenanthrene ring side, as in the case of compound 3, the π - π distance was decreased to 3.333 Å. The π - π distance observed in our previous work for the *n*-perfluorobutyl analogue of compound 3 was 3.400 Å.^{53} By reducing the chain length from n-perfluorobutyl⁵³ to *n*-perfluoropropyl (compound 3, present work), the π - π distance decreased, which was in line with our previous observation, while maintaining the same lamellar packing. Whereas, changing the position of the *n*-perfluoropropyl groups to the 10,13-position in the case of compound 1, the shortest π - π stacking distance of 3.329 Å was observed. Although the shortest interplanar distance was observed in the case of compound 1, the slipped parallel packing motif showed the poorest overlapping among these three isomers (Fig. 1). The network in the crystal packing of compound 1 showed C_{sp2} – $H\cdots$ F– C_{sp3} and $C_{sp2}\cdots$ F– C_{sp3} intermolecular interactions along the b direction. The crystal of compound 2 formed a 3D network through C_{sp3} -F...F- C_{sp3} intermolecular interactions along the c direction. Compound 3 also formed a 3D network through a combination of $C_{\mathrm{sp3}}\text{--}\mathrm{F}\cdots\mathrm{F-}C_{\mathrm{sp3}}$ and C_{sp2} -H···F- C_{sp3} intermolecular interactions along the cdirection.

Hirshfeld surface analysis was used to investigate the different types of intermolecular interactions among all three isomers. From the bar graphs that represent the percentile of different types of intermolecular interactions (Fig. S12†), we can clearly observe that upon changing the n-perfluoropropyl substitution position from compound 1 to compound 3, the contribution of the C···C intermolecular short contacts increased. In the meantime, the amount of the F···C, C···H short contacts decreased. The increase in the $C_{\rm sp3}$ –F··· π (F–C) and $C_{\rm sp2}$ –H··· π (C–H) interactions favoured T-shaped structures, leading to an overall herringbone packing in compound 1. For compound 3, the major dominant short contacts were F···H, F···F, C···H and

Paper CrystEngComm

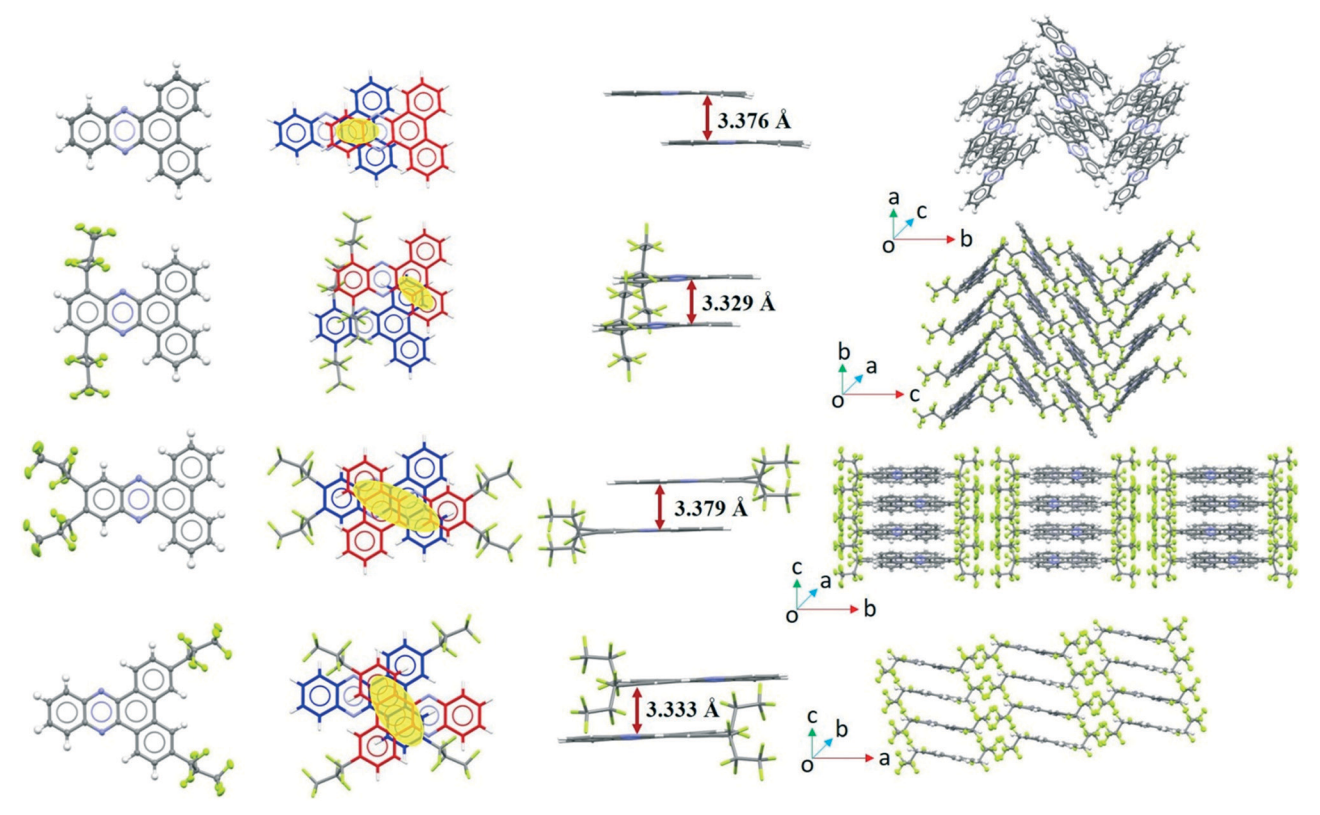


Fig. 1 Crystal structure, top view of the dimer with π overlapping (yellow oval), interplanar distance in the dimers and crystal packing (left to right) of DBP, compounds 1, 2, and 3 (from top to bottom). The interplanar distance was calculated between two adjacent dibenzo[a,c]phenazine molecules with the plane defined by the average of the 22 non-hydrogen atoms of the dibenzo[a,c]phenazine ring.

C···C short contacts. From the 2D fingerprint plots (ESI,† Fig. S9-S11), a clear difference in intermolecular interactions was observed upon changing the substitution position of the *n*-perfluoropropyl group from compound 1 to compounds 2 and 3.

2.3 Effect of the *n*-perfluoropropyl groups' position on the photophysical and electrochemical properties

The UV-visible absorption and emission spectra compounds 1-3 in dilute dichloromethane solution are shown in Fig. 2. The absorption maxima (λ_{max}) compounds 1 and 2 were found to be 404 and 401 nm respectively, whereas for compound 3, the λ_{max} was 389 nm, which was a 15 nm blue-shift in the absorption maximum in

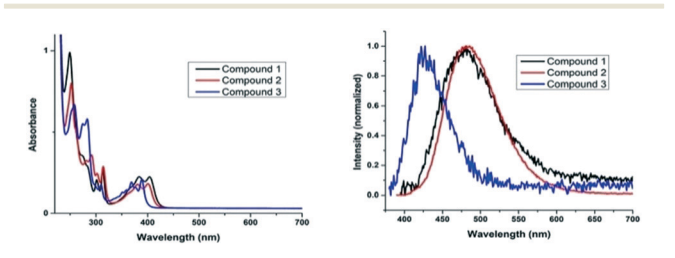


Fig. 2 UV-visible absorption (left) and emission (right) spectra of compounds 1-3 in dichloromethane solution.

comparison to compound 1. The emission maxima for compounds 1 and 2 were 499 and 492 nm respectively, whereas for compound 3, a blue-shift (83 nm) in the emission maximum (416 nm) was observed. The absorption and emission behaviour of these isomers were in good agreement with the calculated band gaps (Table 1).

fundamental electrochemical properties compounds 1-3 were measured by cyclic voltammetry in 1,2-difluorobenzene/0.1 M TBAPF₆ solution (Fig. 3). A reversible first redox couple was observed for all of these three compounds. One-(compounds 1 and 2) or two-(compound 3) irreversible reduction peaks were observed after the first reversible redox couple. The first reversible redox couple represented a single electron-transfer redox process of the phenazine aromatic ring. The substitutional impact of these compounds was reflected by the difference in redox potentials between compounds 1, 2, and 3. Compounds 1 and 2 showed very similar first reduction potentials with less than a 50 mV difference between these two, while compound 3 showed its first reduction potential at a much more negative potential, as shown in Fig. 3. These results were consistent with our electron affinity (EA) calculations (vide infra, Table 1), where compounds 1 and 2 had very similar EA values and both values were higher (easier to be reduced) than that of compound 3.

CrystEngComm **Paper**

Table 1 Change in the electronic properties upon changing the substitution position of the trifluoromethyl group on dibenzo[a,c]phenazine according to the DFT method at the B3LYP/6-311G(d,p) level. IP, ionization potential; EA, electron affinity; λ_h^h , reorganization energy for hole transfer; λ_h^e reorganization energy for electron transfer; DM, dipole moment

Compounds	$E_{\mathrm{HOMO}}/\mathrm{eV}$	$E_{ m LUMO}/{ m eV}$	$E_{\rm Gap}/{\rm eV}$	IP/eV	EA/eV	λ_i^h/eV	λ_i^e/eV	DM/Debye
DBP	-6.27	-2.46	3.81	7.58	1.14	0.280	0.201	0.35
1	-6.62	-3.09	3.53	8.06	1.83	0.210	0.301	2.47
2	-6.71	-3.09	3.62	8.15	1.84	0.220	0.276	6.68
3	-6.82	-2.99	3.83	8.22	1.72	0.222	0.235	5.38

2.4 Effect of the *n*-perfluoropropyl groups' position on the electronic properties: computational approach

The electronic properties of the *n*-perfluoropropyl dibenzo a, c]phenazine isomers were further studied by density functional theory (DFT) at the B3LYP/6-311G(d,p) level of theory in detail. The molecular orbital energy, ionization potential (IP) and electron affinity (EA), and reorganization energy (λ) associated with charge transfer were calculated, as shown in Table 1. Due to the large size of the dibenzo [a,c]phenazine aromatic system, for geometry optimization and the sequential frequency calculations, we chose trifluoromethyl (CF_3) group to represent the n-perfluoropropyl (n-C₃F₇) group, which has a very similar electronic effect.62

The optimized molecular structures of compounds 1-3 from DFT calculations were planar and no twisting of the aromatic rings was observed due to trifluoromethyl groups, which had much less steric effect. Whereas, in the case of the crystal structure of compound 1, moderate twisting was observed due to the reason that one n-perfluoropropyl group faced upward and another n-perfluoropropyl group faced downward, causing steric strain on the aromatic ring. The crystal structures of compounds 2 and 3 maintained a planar structure.

(3.53 eV) and compound 2 (3.62 eV). These results demonstrated fine-tuning potential *n*-perfluoropropyl substituent on the dibenzo[a,c]phenazine molecular orbitals and the corresponding energies through isomerization. Further, we studied the effect of varying the substitution positions of the trifluoromethyl group on the ionization potential, electron affinity, and reorganization energy. From Table 1, it is clear that compounds 1 and 2 had almost the same electron affinity values (1.83 and 1.84 eV), while

The HOMO for compounds 1 and 2 was mainly

concentrated on the side of the phenanthrene ring, which

indicated the donor character (Fig. 4); whereas for compound

3, the HOMO was located on the overall phenazine ring. The

large delocalization of the HOMO in compound 3 provided

further stabilization energy, resulting in compound 3

possessing the lowest HOMO energy among these phenazine

isomers. The LUMO was located over the central phenazine

ring in all three isomers (Fig. 4). Compound 3 had a relatively

lower HOMO energy (-6.82 eV) compared to compounds 1

(-6.62 eV) and 2 (-6.71 eV). The LUMO energy for compounds

1 and 2 were the same (-3.09 eV), while the LUMO energy for

compound 3 was higher (-2.99 eV) compared to compounds

1 and 2 (Table 1). The HOMO-LUMO energy gap was much

higher for compound 3 (3.83 eV) compared to compound 1

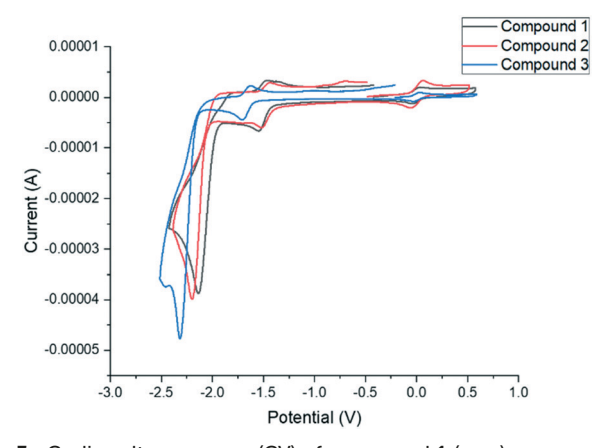


Fig. 3 Cyclic voltammogram (CV) of compound 1 (grey), compound 2 (red), compound 3 (blue) at 100 mV s⁻¹ potential sweep rate in 0.1 M TBAPF₆/1,2-difluorobenzene solution. The potential was corrected with the Fc/Fc⁺ redox couple (shown as the reversible redox couple at 0.0 V in the figure) by adding ferrocene into the solution during the electrochemistry experiments.

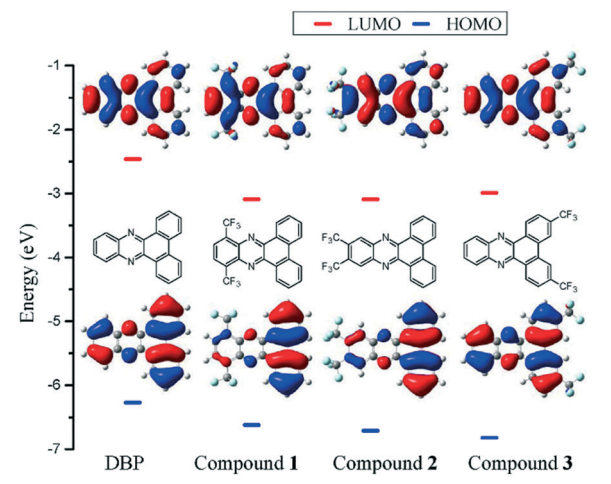


Fig. 4 Changes in HOMO, LUMO energy upon changing the substitution position of trifluoromethyl group on dibenzo[a,c] phenazine with comparison to non-substituted dibenzo[a,c]phenazine

Paper CrystEngComm

compound 3 had a lower electron affinity value (1.72 eV), indicating that compound 1 and 2 were easier to be reduced compared to compound 3. The calculated ionization potentials from Table 1 showed that compound 3 had the highest ionization potential value (8.22 eV) compared to compound 2 (8.18 eV) and compound 1 (8.06 eV), indicating that compound 3 was more difficult to be oxidized among all three isomers in this study. From Table 1, the reorganization energy for electron transfer (ET) for compound 3 was the lowest among all three trifluoromethylated phenazine isomers, and it was very close to DBP (non-substituted phenazine). The reorganization energy for hole transfer for compound 3 (0.222 eV) was close to that for electron transfer (0.235 eV). These results suggest that by varying the substitution positions of the trifluoromethyl group on dibenzo[a,c]phenazine, the electronic properties could potentially be tuned.

It was not surprising that a higher dipole moment was observed for compound 2 (6.68) followed by compound 3 (5.38) and the least for compound 1 (2.47) due to the different positions of the highly electron-withdrawing trifluoromethyl groups on the phenazine ring. In compounds 2 and 3, both trifluoromethyl groups work together with their local dipole cumulate together to amplify the dipole of the entire molecule. The two local dipole moments generated by trifluoromethyl substituents on the opposite position of the phenazine ring in the case of compound 1 cancel out; however, their electron-withdrawing effect still changes the electron density of the local phenyl ring they are attached to, making the phenyl ring more electron deficient. This resulted in a moderate overall dipole moment for compound 1 compared to DBP (non-substituted phenazine).

The change in the n-perfluoropropyl substitution position further altered the electrostatic potential (ESP) distribution among the phenazine surface (Fig. 5). As shown in Fig. 5, the ESP maps indicated that perfluoropropylation makes the aromatic ring more electron deficient in general compared to non-substituted phenazine (DBP),63 while compound 1

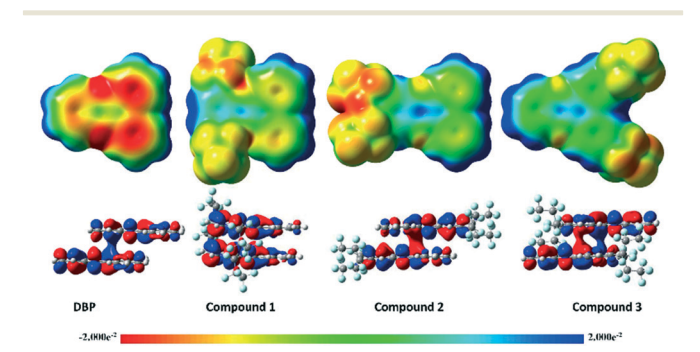


Fig. 5 Comparison of the electrostatic potential (ESP) maps mapped on the total electron density for compounds 1-3 and the corresponding non-substituted dibenzo[a,c]phenazine (DBP) calculated with the M06-2x/TZVP method and basis set. Initial geometries were taken from the crystal structures and calculated single point energy. The colour scale bar at the bottom of the figure is for the relative ESP maps shown in this figure.

showed a moderate increase in electron deficiency on the ring. Compounds 2 and 3 showed greater electron deficiency on the phenazine ring compared to that of compound 1, while compound 3 was slightly more electron deficient than compound 2. Further, the ESP maps clearly showed the steric hindrance of the two *n*-perfluoropropyl groups when they reside next to each other on two adjacent carbon atoms of the phenyl ring. As expected, two nitrogen atoms within the phenazine ring provide large unevenly electrostatic potential on the phenazine surface, which helped maximize the electrostatic interactions in the dimer molecules.

"steering effect" effect Together with the of *n*-perfluoropropyl groups, this unevenly distributed ESP along the aromatic surface assisted building a lamellar π - π stacked crystal packing for compounds 2 and 3. However, for compound 1, the localized electron-rich regions caused by nitrogen atoms overlapped with the n-perfluoropropyl groups, resulting in a blocking effect stopping another phenazine ring from overlapping with it to a greater extent.

The dimer interaction energies among the dimers of compounds 1-3 were calculated computationally using the crystal structure with the M06-2X/TZVP method and basis set with BSSE correction. 64-66 Similar dimerization energies for compound 2 (-17.2 kcal mol⁻¹) and compound 3 (-16.4 kcal mol⁻¹) were observed, and both of them were much higher than that of compound 1 (-12.8 kcal mol⁻¹), which is in line with the ESP maps (Fig. 5) and crystal packing discussed earlier (Fig. 1).

Again, compound 3 had a relatively similar LUMO overlapping (Fig. 5) to that of compound 2; while there was almost no LUMO overlapping for compound 1 due to the very small overlapping area in its crystal packing. No HOMO overlapping was observed for the dimers of all three isomers in this study. These results suggest that the presence of *n*-perfluoropropyl groups on the 3,6-positions of dibenzo[a,c] phenazine provide ideal lamellar crystal packing with effective π overlapping and a smaller interplanar distance.

3 Conclusions

In summary, we successfully prepared and characterized three n-perfluoropropyl dibenzo[a,c]phenazine isomers, where the only difference was the position of *n*-perfluoropropyl group substitution. We observed that the crystal packing motifs in these three isomers were changed from herringbone with minimum π system overlapping to perfect lamellar with much better π system overlapping by simply changing the substitution position of the *n*-perfluoropropyl groups on the dibenzo [a,c] phenazine ring. Our computational chemistry results showed that changing the *n*-perfluoropropyl substituent position not only changed the steric hindrance on the perpendicular direction of the π system but also drastically changed the electrostatic potential distribution for the corresponding π system. As exemplified by the solid-state

CrystEngComm Paper

structure of compound 3, a cooperative relationship between the enhanced electrostatic interaction between π systems and reduced steric hindrance of the perfluoroalkyl substituents on the same π system is likely one of the key factors in the formation of a perfect lamellar packing motif in perfluoroalklyated polyaromatics. Finally, the redox potential, electronic spectra, and DFT calculation results were consistent; together pointing out that there were only minor to moderate changes in the electronic properties of the position changing molecules upon the perfluoroalkylation on the dibenzo [a,c] phenazine ring, while the solid-state structures of these constitutional isomers were significantly different. With that, we can reasonably predict that one can possibly tune the solid-state structure of an semiconductor by simply changing perfluoroalkylation position, yet without significantly altering the electronic properties of the semiconductor core.

4 Experimental section

General

All chemicals and solvents were purchased from commercial sources and used as received. NMR spectra were collected using CDCl₃ as the solvent. ¹H and ¹⁹F NMR spectra were recorded on a Bruker Avance III HD 400 MHz NMR spectrometer and the chemical shifts were reported in parts per million (ppm). Mass spectra were recorded on GC-2010 plus Shimadzu, Varian 500-MS, Scientific QExactive Plus orbitrap spectrometers with EI and ESI techniques. Elemental analyses were carried out using an Exeter Analytic (CE-440) system with helium as the carrier gas. Crystallographic data were recorded on a Bruker D8 Venture system using Mo K α radiation ($\lambda = 0.71073$ Å) at 100 K and the data were integrated using Apex III software. Crystal structures were solved using the SHELXT and WinGX packages. All non-hydrogen atoms were refined anisotropically and all hydrogen atoms were treated isotropically. Images of the crystal structures and crystal packing were produced using Mercury 4.3.1. Hirshfeld surface analysis was carried out using Crystal Explorer 17.5 and the percentage contribution of short contacts was determined from 2D finger print plots. 67,68

UV-visible spectral studies were carried out using a Cary 5000 UV-Vis-NIR spectrophotometer (Varian Inc.). Fluorescence spectra were collected using a Fluoromax-4 spectrofluorometer (Horiba Jobin Yvon). Cyclic voltammetry (CV) experiments were performed using an Autolab P302N potentiostat/galvanostat with Nova 2.0 software. The electrochemical cell consisted of a glassy carbon disc electrode (3 mm diameter) as the working electrode, Pt wire as the counter electrode, and Ag/AgCl electrode as a quasi-reference electrode. 1,2-Difluorobenzene (DFB) (dried over flame-dried 4A MS) with 0.1 M tetrabutylammonium hexafluorophosphate (TBAPF₆) was used as the electrolyte solution for all the electrochemical experiments. All CV

Table 2 Summary of the crystal data, data collection, and structure refinement parameters for 10, 13-dibromo-dibenzo[a,c]phenazine (PBrDBP), compound 1 and compound 3 with CCDC deposition numbers 2053442-2053444 respectively. Crystal structure of PBrDBP is provided in the ESI.† Compound 2 structure was published with a CCDC deposition number 968257

		Compound	Compound
	PBrDBP	1	3
CCDC#	2053442	2053443	2053444
Formula	$C_{20}H_{10}Br_2N_2$	$C_{26}H_{10}F_{14}N_2$	$C_{26}H_{10}F_{14}N_2$
Formula wt	438.12	616.36	616.36
Temp, K	100	100	100
Crystal setting	Orthorhombic	Monoclinic	Monoclinic
Space group	P212121	P21/c	C2/c
Hall symbol	-P 2 ac 2ab	−P 2ybc	-C 2yc
International tables#	19	14	15
a, Å	4.2682	16.0011	23.9534
b, Å	18.1897	5.2318	13.3698
c, Å	19.6942	27.377	7.2037
α , deg	90	90	90
β , deg	90	101.533	93.922
γ, deg	90	90	90
z	4	4	4
Cell volume(ų)	1529.00	2245.6	2301.6
Density, g cm ⁻³	1.903	1.823	1.779
Ab coefficient, mm ⁻¹	5.304	0.190	0.185
F(000)	856.0	1224	1224
Data range $(\theta_{\min} - \theta_{\max})$	2.35-31.32	2.19-25.98	2.98-34.33
Index ranges	$\pm 7, \pm 31, \pm 33$	$\pm 19, \pm 6, \pm 33$	$\pm 37, \pm 21,$
			±11
Measured reflections	26 358	38 876	30 658
Independent reflections	8214	4440	4856
Reflections with $I >$	5153	3383	3129
$2\sigma(I)$			
Max/Min trans	0.400/0.620	0.982/0.989	0.985/0.974
Restraints/Parameters	0/217	0/379	0/190
GOF	0.924	1.135	1.020
$R\left[F^2>2\sigma(F^2)\right]$	0.0407	0.0483	0.0533
$WR(F^2)$	0.0847	0.1221	0.1581

experiments were carried out inside an argon-filled glove box with the $\rm O_2$ and $\rm H_2O$ levels controlled at less than 0.1 ppm. The Fc/Fc $^+$ redox couple was used to correct the final reported redox potential. All the computational calculations were performed using the Gaussian 16 software; and GaussView 6.0 was used for processing the computational chemistry results. 69,70

The detailed synthetic procedures and characterization data for compounds 1 and 3, as well as the detailed computational chemistry procedures are provided in the ESI.†

Crystallographic data

See Table 2.

Author contributions

H. S. and A. P. conceptualized and outlined the manuscript. A. P. synthesized and characterized compound 1, collected single-crystal XRD data, solved crystal structures, and performed computational study. S. G. synthesized and

Paper CrystEngComm

characterized compound 3, and measured photophysical properties. Y. F. measured and analysed electrochemistry results. A. P. wrote the original draft of the manuscript and revised it with input from all authors. H. S. and A. P. finalized the manuscript. H. S. provided funding support through both federal and state grant agencies as listed in the acknowledgement section.

Conflicts of interest

Authors declare no competing financial interests.

Acknowledgements

Authors like to thank the U.S. Army Research Office (W911NF-09-10472) and the NSF (CHE1355677) for funding supports. Financial support from the South Dakota Governor's Office of Economic Development through the Center for Fluorinated Functional Materials are also appreciated. Bruker Dual Source Single-Crystal X-ray Diffractometer purchase was possible by funding from an NSF-MRI grant CHE-1919637. The authors like to thank the University of South Dakota Lawrence High-Performance Computing facility and the NSF (grant number: ACI-1626516) for providing computational resources. The authors thank Dr. Eduardo Callegari for assistance in acquiring mass spectra for compound 3.

Notes and references

- 1 X. Zhang, H. Dong and W. Hu, Adv. Mater., 2018, 30, 1801048.
- 2 P. Yu, Y. Zhen, H. Dong and W. Hu, *Chem*, 2019, 5, 2814–2853.
- 3 Q. Li and Z. Li, Acc. Chem. Res., 2020, 53, 962-973.
- 4 C. Sutton, C. Risko and J.-L. Brédas, *Chem. Mater.*, 2016, 28, 3–16.
- 5 S. Tsuzuki, K. Honda, T. Uchimaru, M. Mikami and K. Tanabe, *J. Am. Chem. Soc.*, 2002, **124**, 104–112.
- 6 S. Tsuzuki, K. Honda, T. Uchimaru, M. Mikami and K. Tanabe, *J. Am. Chem. Soc.*, 2000, **122**, 3746–3753.
- 7 M. M. Payne, S. R. Parkin and J. E. Anthony, *J. Am. Chem. Soc.*, 2005, **127**, 8028–8029.
- 8 J. E. Anthony, Chem. Rev., 2006, 106, 5028-5048.
- S. A. Sharber, R. N. Baral, F. Frausto, T. E. Haas, P. Müller and S. W. Thomas Iii, J. Am. Chem. Soc., 2017, 139, 5164–5174.
- 10 P. S. Salini, S. K. Rajagopal and M. Hariharan, Cryst. Growth Des., 2016, 16, 5822–5830.
- 11 Monika, A. Verma, M. K. Tiwari, B. Show and S. Saha, ACS Omega, 2020, 5, 448–459.
- 12 K. E. Maly, Cryst. Growth Des., 2011, 11, 5628-5633.
- 13 U. H. F. Bunz, Acc. Chem. Res., 2015, 48, 1676-1686.
- 14 T. Higashino, S. Arai, S. Inoue, S. Tsuzuki, Y. Shimoi, S. Horiuchi, T. Hasegawa and R. Azumi, *CrystEngComm*, 2020, 22, 3618–3626.
- 15 T. Schmaltz, B. Gothe, A. Krause, S. Leitherer, H.-G. Steinrück, M. Thoss, T. Clark and M. Halik, *ACS Nano*, 2017, 11, 8747–8757.

16 H. Chen, W. Zhang, M. Li, G. He and X. Guo, *Chem. Rev.*, 2020, 120, 2879–2949.

- 17 A. de Bettencourt-Dias, S. Viswanathan and K. Ruddy, *Cryst. Growth Des.*, 2005, 5, 1477–1483.
- 18 N. Demir, G. Yakali, M. Karaman, Y. Gokpek, S. Denizalti, H. Bilgili, B. Dindar, S. Demic and M. Can, *J. Phys. Chem. C*, 2019, **123**, 21998–22008.
- 19 J.-H. Dou, Y.-Q. Zheng, Z.-F. Yao, Z.-A. Yu, T. Lei, X. Shen, X.-Y. Luo, J. Sun, S.-D. Zhang, Y.-F. Ding, G. Han, Y. Yi, J.-Y. Wang and J. Pei, *J. Am. Chem. Soc.*, 2015, 137, 15947–15956.
- 20 D. Tian, Z. Ma, L. Gu, C. Zhou, C. Li, Z. Wang and H. Wang, Cryst. Growth Des., 2020, 20, 4479–4490.
- 21 A. K. Hailey, A. J. Petty Ii, J. Washbourne, K. J. Thorley, S. R. Parkin, J. E. Anthony and Y.-L. Loo, *Adv. Mater.*, 2017, 29, 1700048.
- 22 R. Bu, F. Jiao, G. Liu, J. Zhao and C. Zhang, *Cryst. Growth Des.*, 2021, 21, 3–15.
- 23 Q. Yue, Y.-Y. Wang, X.-L. Hu, W.-X. Guo and E.-Q. Gao, *CrystEngComm*, 2019, **21**, 6719–6732.
- 24 Q. Zhang, D. Chen, X. He, S. Huang, J. Huang, X. Zhou, Z. Yang, J. Li, H. Li and F. Nie, *CrystEngComm*, 2014, 16, 10485–10491.
- 25 Y. Shang, R.-K. Huang, S.-L. Chen, C.-T. He, Z.-H. Yu, Z.-M. Ye, W.-X. Zhang and X.-M. Chen, *Cryst. Growth Des.*, 2020, 20, 1891–1897.
- 26 G. R. Desiraju, Acc. Chem. Res., 2002, 35, 565-573.
- 27 P. Gómez, S. Georgakopoulos, M. Más-Montoya, J. Cerdá, J. Pérez, E. Ortí, J. Aragó and D. Curiel, ACS Appl. Mater. Interfaces, 2021, 13, 8620–8630.
- 28 J. Luo, J.-W. Wang, J.-H. Zhang, S. Lai and D.-C. Zhong, *CrystEngComm*, 2018, **20**, 5884–5898.
- 29 A. Priimagi, G. Cavallo, P. Metrangolo and G. Resnati, *Acc. Chem. Res.*, 2013, 46, 2686–2695.
- 30 Y. Sakamoto and T. Suzuki, *J. Org. Chem.*, 2017, **82**, 8111–8116.
- 31 K. Merz, M. V. Evers, F. Uhl, R. I. Zubatyuk and O. V. Shishkin, *Cryst. Growth Des.*, 2014, 14, 3124–3130.
- 32 S. Tsuzuki, Annu. Rep. Prog. Chem., Sect. C: Phys. Chem., 2012, 108, 69-95.
- 33 P. Panini and D. Chopra, *CrystEngComm*, 2012, 14, 1972–1989.
- 34 M. K. Ravva, C. Risko and J.-L. Brédas, in *Non-Covalent Interactions in Quantum Chemistry and Physics*, ed. A. Otero de la Roza and G. A. DiLabio, Elsevier, 2017, pp. 277–302, DOI: 10.1016/B978-0-12-809835-6.00011-6.
- 35 M. K. Corpinot and D.-K. Bučar, *Cryst. Growth Des.*, 2019, 19, 1426–1453.
- 36 S. J. Nam, S. J. Jeon, Y. W. Han and D. K. Moon, *J. Ind. Eng. Chem.*, 2018, **63**, 191–200.
- 37 H. Usta, A. Facchetti and T. J. Marks, *Acc. Chem. Res.*, 2011, 44, 501–510.
- 38 D. M. Cho, S. R. Parkin and M. D. Watson, *Org. Lett.*, 2005, 7, 1067–1068.
- 39 K. P. Castro, T. T. Clikeman, N. J. DeWeerd, E. V. Bukovsky, K. C. Rippy, I. V. Kuvychko, G.-L. Hou, Y.-S. Chen, X.-B.

CrystEngComm **Paper**

Wang, S. H. Strauss and O. V. Boltalina, Chem. - Eur. J., 2016, 22, 3930-3936.

- 40 L. Pilia, Y. Shuku, S. Dalgleish, D. W. M. Hofmann, N. Melis, K. Awaga and N. Robertson, J. Organomet. Chem., 2020, 918, 121277
- 41 R. Schmidt, J. H. Oh, Y.-S. Sun, M. Deppisch, A.-M. Krause, K. Radacki, H. Braunschweig, M. Könemann, P. Erk, Z. Bao and F. Würthner, J. Am. Chem. Soc., 2009, 131, 6215-6228.
- 42 Y. Li, L. Tan, Z. Wang, H. Qian, Y. Shi and W. Hu, Org. Lett., 2008, 10, 529-532.
- 43 R. K. Radha Krishnan, B. J. Reeves, S. H. Strauss, O. V. Boltalina and B. Lüssem, Org. Electron., 2020, 86, 105898.
- 44 S. Yamada, K. Kinoshita, S. Iwama, T. Yamazaki, T. Kubota, T. Yajima, K. Yamamoto and S. Tahara, Org. Biomol. Chem., 2017, 15, 2522-2535.
- 45 W. Cao and E. M. Sletten, J. Am. Chem. Soc., 2018, 140, 2727-2730.
- 46 H. Sun, A. Putta, J. P. Kloster and U. K. Tottempudi, Chem. Commun., 2012, 48, 12085-12087.
- 47 Z. Zhang, J. Xiong, G. He, D. Dang, Y. Xie and Q. Wang, Polym. Chem., 2020, 11, 1307-1313.
- 48 I. Shulov, S. Oncul, A. Reisch, Y. Arntz, M. Collot, Y. Mely and A. S. Klymchenko, Nanoscale, 2015, 7, 18198-18210.
- 49 B. A. Jones, A. Facchetti, M. R. Wasielewski and T. J. Marks, J. Am. Chem. Soc., 2007, 129, 15259-15278.
- 50 H. Sun, A. Putta and M. Billion, J. Phys. Chem. A, 2012, 116, 8015-8022.
- 51 A. Putta, J. D. Mottishaw, Z. Wang and H. Sun, Cryst. Growth Des., 2014, 14, 350-356.
- 52 H. Sun, U. K. Tottempudi, J. D. Mottishaw, P. N. Basa, A. Putta and A. G. Sykes, Cryst. Growth Des., 2012, 12, 5655-5662.
- 53 M. O. BaniKhaled, J. D. Mottishaw and H. Sun, Cryst. Growth Des., 2015, 15, 2235-2242.
- 54 Z.-H. Guo, T. Lei, Z.-X. Jin, J.-Y. Wang and J. Pei, Org. Lett., 2013, 15, 3530-3533.
- 55 Y. Liu, Y. Chen, H. Li, S. Wang, X. Wu, H. Tong and L. Wang, ACS Appl. Mater. Interfaces, 2020, 12, 30652-30658.
- 56 J. Shi, J. Chen, Z. Chai, H. Wang, R. Tang, K. Fan, M. Wu, H. Han, J. Qin, T. Peng, Q. Li and Z. Li, J. Mater. Chem., 2012, 22, 18830-18838.
- 57 H. Deol, G. Singh, M. Kumar and V. Bhalla, J. Org. Chem., 2020, 85, 11080-11093.

- 58 M. Li, C. An, T. Marszalek, X. Guo, Y.-Z. Long, H. Yin, C. Gu, M. Baumgarten, W. Pisula and K. Müllen, Chem. Mater., 2015, 27, 2218-2223.
- 59 P. K. Sahoo, C. Giri, T. S. Haldar, R. Puttreddy, K. Rissanen and P. Mal, Eur. J. Org. Chem., 2016, 2016, 1283-1291.
- 60 Y. Yang, A. Li, Z. Ma, J. Liu, W. Xu, Z. Ma and X. Jia, Dyes Pigm., 2020, 181, 108575.
- 61 M. O. BaniKhaled, J. D. Becker, M. Koppang and H. Sun, Cryst. Growth Des., 2016, 16, 1869-1878.
- 62 C. Hansch, A. Leo and R. W. Taft, Chem. Rev., 1991, 91, 165-195.
- 63 M. W. Day, X. A. Amashukeli and H. B. Gray, CSD Communication, 2002, DOI: 10.5517/cc4rt0p.
- 64 Y. Zhao and D. G. Truhlar, Theor. Chem. Acc., 2008, 120, 215-241.
- 65 A. Schäfer, C. Huber and R. Ahlrichs, J. Chem. Phys., 1994, 100, 5829-5835.
- 66 J. B. Foresman and A. E. Frisch, Exploring Chemistry with Electronic Structure Methods, Gaussian, Inc., Wallingford, CT, 2015.
- 67 M. A. Spackman and D. Jayatilaka, CrystEngComm, 2009, 11, 19-32.
- 68 M. A. Spackman and J. J. McKinnon, CrystEngComm, 2002, 4, 378-392.
- 69 M. J. Frisch, G. W. Trucks, H. B. Schlegel, G. E. Scuseria, M. A. Robb, J. R. Cheeseman, G. Scalmani, V. Barone, G. A. Petersson, H. Nakatsuji, X. Li, M. Caricato, A. V. Marenich, J. Bloino, B. G. Janesko, R. Gomperts, B. Mennucci, H. P. Hratchian, J. V. Ortiz, A. F. Izmaylov, J. L. Sonnenberg, F. Ding Williams, F. Lipparini, F. Egidi, J. Goings, B. Peng, A. Petrone, T. Henderson, D. Ranasinghe, V. G. Zakrzewski, J. Gao, N. Rega, G. Zheng, W. Liang, M. Hada, M. Ehara, K. Toyota, R. Fukuda, J. Hasegawa, M. Ishida, T. Nakajima, Y. Honda, O. Kitao, H. Nakai, T. Vreven, K. Throssell, J. A. Montgomery Jr., J. E. Peralta, F. Ogliaro, M. J. Bearpark, J. J. Heyd, E. N. Brothers, K. N. Kudin, V. N. Staroverov, T. A. Keith, R. Kobayashi, J. Normand, K. Raghavachari, A. P. Rendell, J. C. Burant, S. S. Iyengar, J. Tomasi, M. Cossi, J. M. Millam, M. Klene, C. Adamo, R. Cammi, J. W. Ochterski, R. L. Martin, K. Morokuma, O. Farkas, J. B. Foresman and D. J. Fox, Gaussian 16, Rev. C.01, Gaussian, Inc., Wallingford CT, 2016.
- 70 R. Dennington, T. A. Keith and J. M. Millam, GaussView 6.0, Semichem Inc., Shawnee Mission, KS, 2016.